Polarization states of polydomain epitaxial Pb(Zr$_{1-x}$Ti$_x$)O$_3$ thin films and their dielectric properties

V. G. Kukhar,[1] N. A. Pertsev,[2,3,*] H. Kohlstedt,[2,4] and R. Waser[2,5]

[1]*Scientific Research Institute "Vector", St. Petersburg, Russia*
[2]*Institut für Festkörperforschung and CNI, Forschungszentrum Jülich, D-52425 Jülich, Germany*
[3]*A. F. Ioffe Physico-Technical Institute, Russian Academy of Sciences, 194021 St. Petersburg, Russia*
[4]*Department of Material Science and Engineering and Department of Physics,*
University of California, Berkeley, California 94720, USA
[5]*Institut für Werkstoffe der Elektrotechnik, RWTH Aachen University of Technology, D-52056 Aachen, Germany*

Ferroelectric and dielectric properties of polydomain (twinned) single-crystalline Pb(Zr$_{1-x}$Ti$_x$)O$_3$ thin films are described with the aid of a nonlinear thermodynamic theory, which has been developed recently for epitaxial ferroelectric films with dense laminar domain structures. For Pb(Zr$_{1-x}$Ti$_x$)O$_3$ (PZT) films with compositions $x=0.9$, 0.8, 0.7, 0.6, 0.5, and 0.4, the "misfit strain-temperature" phase diagrams are calculated and compared with each other. It is found that the equilibrium diagrams of PZT films with $x \geqslant 0.7$ are similar to the diagram of PbTiO$_3$ films. They consist of only four different stability ranges, which correspond to the paraelectric phase, single-domain tetragonal ferroelectric phase, and two pseudotetragonal domain patterns. In contrast, at $x=0.4$, 0.5, and 0.6, the equilibrium diagram displays a rich variety of stable polarization states, involving at least one *monoclinic* polydomain state. Using the developed phase diagrams, the mean out-of-plane polarization of a poled PZT film is calculated as a function of the misfit strain and composition. Theoretical results are compared with the measured remanent polarizations of PZT films grown on SrTiO$_3$. Dependence of the out-of-plane dielectric response of PZT films on the misfit strain in the heterostructure is also reported.

I. INTRODUCTION

Among the broad range of ferroelectric materials, solid solutions like Pb(Zr$_{1-x}$Ti$_x$)O$_3$ and (Ba$_x$Sr$_{1-x}$)TiO$_3$ represent an object of special interest because their physical properties can be tuned by changing the chemical composition. Nowadays, these ferroelectrics are mostly studied in a thin-film form, which is favorable for various device applications. In particular, thin films of Pb(Zr$_{1-x}$Ti$_x$)O$_3$ (PZT) have been fabricated in many laboratories worldwide, and even epitaxial PZT films were grown on many different substrates.[1–13] The experimental results demonstrated several important distinctions between the properties of PZT in a thin film and bulk forms, which triggered the first theoretical studies of PZT thin films.[14–17] Two approaches were employed in these studies, namely, the thermodynamic calculations and the phase-field simulations. Although the latter approach has some advantages in the description of equilibrium polarization states of ferroelectric films,[17,18] the thermodynamic calculations still represent the only way to determine the dielectric and piezoelectric properties of these films.[15,19,20]

In our preceding paper,[15] we developed the thermodynamic theory of epitaxial PZT thin films under the assumption that only single-domain ferroelectric states form in these films. The "misfit strain-temperature" phase diagrams of single-domain PZT films were constructed, and their small-signal dielectric and piezoelectric responses calculated as a function of the misfit strain in the film-substrate system.[15] Since in epitaxial ferroelectric films the polydomain (twinned) states are often energetically favored over single-domain states,[21–24] further development of our thermodynamic theory calls for a description of the domain formation

in PZT films. In this paper, we focus on dense laminar domain structures, where the domain widths are much smaller than the film thickness (but large enough to neglect self-energies of domain walls in comparison with the energy stored inside domains). Such polydomain states are expected to form in PZT films with a conventional thickness (~100 nm and larger) and can be described with the aid of a Landau-Ginsburg-Devonshire-type nonlinear theory.[20] In Sec. II, we briefly discuss the method of thermodynamic calculations proposed in Ref. 20, which makes it possible to determine the polarization configuration in a ferroelectric film with a dense domain structure and to evaluate the film free energy. Section III reports the equilibrium misfit strain-temperature phase diagrams of PZT films (with the Ti content $x=0.9$, 0.8, 0.7, 0.6, 0.5, and 0.4), which were constructed by numerically calculating the energies of various polydomain and single-domain states and comparing them with each other. The lattice strains and unit-cell distortions in ferroelastic domains of different types are discussed in Sec. IV. In Sec. V we describe the small-signal dielectric response of epitaxial PZT films. The most important conclusions, which follow from the performed theoretical investigations, are formulated in Sec. VI.

II. THERMODYNAMICS OF PZT FILMS WITH DENSE DOMAIN STRUCTURES

When the domain structure has the form of an array of flat domain walls parallel to each other and separated by distances much smaller than the film thickness, the polarization and lattice strains become nearly uniform within each domain in the major part of the film volume.[20] The distribution

of the energy density in this inner region of a polydomain film is, therefore, practically piecewise homogeneous. The theoretical analysis shows that the total free energy of the film/substrate system may be approximately set equal to the energy stored inside the region of "piecewise homogeneity."[20] Moreover, the self-energy of domain walls may be neglected in comparison with the energy of domains, if there is no need to calculate the density of domain walls in the film. (The equilibrium density can be evaluated in the linear elastic approximation by assuming the laminar domain structure to be periodic.[24] The calculation shows that this density is small enough to neglect the domain-wall energies even at the minimum film thickness ~ 100 nm considered in this paper.)

Since the polarization and lattice strains vary from one domain to another in a polydomain film, we cannot use the thin-film thermodynamic potential[19,15] for the determination of equilibrium multidomain states. Instead, we shall employ the general thermodynamic approach based on the calculation of the total Helmholtz free energy of the system and the work done by external forces. In the usual case of a film-substrate system with a mechanically free outer surface, the external mechanical forces are zero so that the total energy can be evaluated by integrating the Helmholtz free-energy density $\widetilde{F}$ over the volume of this system.[20] For a film with a dense laminar domain structure, the total energy is determined by the product of the mean energy density $\langle\widetilde{F}\rangle$ in the inner region of a polydomain layer and the film volume. The density $\langle\widetilde{F}\rangle$ can be written as $\langle\widetilde{F}\rangle = \phi\widetilde{F}' + (1-\phi)\widetilde{F}''$, where $\widetilde{F}'$ and $\widetilde{F}''$ are the characteristic energy densities inside domains of the first and second type, and $\phi' = \phi$ and $\phi'' = 1 - \phi$ are their volume fractions in the film.

The energy density $\widetilde{F}$ is defined by the relation $\widetilde{F} = F - E_i(\epsilon_0 E_i + P_i)$, where F is the usual Helmholtz energy density, E_i $(i=1,2,3)$ are the components of internal electric field in the film, P_i are the polarization components, ε_0 is the permittivity of the vacuum, and the summation over the repeated index i is implied. Since only the Gibbs free energy function G is known for PZT,[25] we shall derive the energy F via the inverse Legendre transformation of G. This procedure yields $F = G + \sigma_{ij}S_{ij} = G_0 + \sigma_{ij}S_{ij} - \frac{1}{2}s_{ijkl}\sigma_{ij}\sigma_{kl} - Q_{ijkl}\sigma_{ij}P_kP_l$, where G_0 is the six-degree polynomial in P_i,[25] σ_{ij} are the mechanical stresses, S_{ij} are the lattice strains, s_{ijkl} are the elastic compliances at constant polarization, and Q_{ijkl} are the electrostrictive constants in the full polarization notation. The equations of state $S_{ij} = -\partial G/\partial\sigma_{ij}$ enable us to eliminate the strains from the above formula. Using the Voigt matrix notation and the reference frame (x_1, x_2, x_3) of the prototypic cubic phase, we then obtain the following expression for the energy density $\widetilde{F}$:

$$\widetilde{F} = \alpha_1(P_1^2 + P_2^2 + P_3^2) + \alpha_{11}(P_1^4 + P_2^4 + P_3^4) + \alpha_{12}(P_1^2P_2^2 + P_1^2P_3^2$$
$$+ P_2^2P_3^2) + \alpha_{111}(P_1^6 + P_2^6 + P_3^6) + \alpha_{112}[P_1^4(P_2^2 + P_3^2) + P_2^4(P_1^2$$
$$+ P_3^2) + P_3^4(P_1^2 + P_2^2)] + \alpha_{123}P_1^2P_2^2P_3^2 + \frac{1}{2}s_{11}(\sigma_1^2 + \sigma_2^2 + \sigma_3^2)$$

$$+ s_{12}(\sigma_1\sigma_2 + \sigma_1\sigma_3 + \sigma_2\sigma_3) + \frac{1}{2}s_{44}(\sigma_4^2 + \sigma_5^2 + \sigma_6^2)$$

$$- \frac{1}{2}\epsilon_0(E_1^2 + E_2^2 + E_3^2) - E_1P_1 - E_2P_2 - E_3P_3, \quad (1)$$

where α_1, α_{ij}, and α_{ijk} are the dielectric stiffness and higher-order stiffness coefficients at constant stress. It should be emphasized that the stresses σ_n in Eq. (1) are not regarded as independent parameters; these internal stresses are coupled to the polarization components and lattice strains by the equations of state involving electrostrictive terms (see below). We also note that the eighth-order polarization terms, which are required for the description of unusual monoclinic phase in bulk PZT,[26] are neglected here because the sixth-order theory is expected to be sufficient in the case of epitaxial thin films.[15] The energy contributions associated with the tilting of the oxygen octahedra and the antiferroelectric-type polarization were also ignored in Eq. (1). This approximation is fairly good in the range of compositions $(x \geqslant 0.4)$ and temperatures $(T \geqslant 0\ ^\circ\text{C})$, which are considered in this paper.[15]

The equilibrium polarization state of a polydomain film can be found via the minimization of the mean energy density $\langle\widetilde{F}\rangle$. If the orientation of domain walls is assumed to be predetermined, the minimization procedure enables us to calculate the polarization components P_i' and P_i'' in the domains of two types and the equilibrium domain population ϕ. In order to make this calculation possible, it is necessary to eliminate internal stresses σ_n', σ_n'' and electric fields E_i', E_i'' from the general expression for $\langle\widetilde{F}\rangle$, which results from Eq. (1). This problem can be solved by using the mechanical and electric boundary conditions imposed on a polydomain epitaxial layer. Restricting our analysis to PZT films grown in the (001)-oriented paraelectric state on the (001) face of a thick cubic substrate, from the epitaxial relationship we obtain the mean in-plane film strains to be $\langle S_1\rangle = \langle S_2\rangle = S_m$ and $\langle S_6\rangle = 0$, where S_m is the misfit strain in the film-substrate system (see Ref. 15). The elastic equation of state of a ferroelectric crystal makes it possible to express the relevant strains as

$$S_1 = s_{11}\sigma_1 + s_{12}(\sigma_2 + \sigma_3) + Q_{11}P_1^2 + Q_{12}(P_2^2 + P_3^2), \quad (2)$$

$$S_2 = s_{11}\sigma_2 + s_{12}(\sigma_1 + \sigma_3) + Q_{11}P_2^2 + Q_{12}(P_1^2 + P_3^2), \quad (3)$$

$$S_6 = s_{44}\sigma_6 + Q_{44}P_1P_2, \quad (4)$$

where Q_{mn} are the electrostrictive constants in the matrix notation. Accordingly, the epitaxial relationship gives us three equations for the stresses σ_n', σ_n'' in a polydomain film. The absence of tractions acting on the upper surface of the film yields three additional equations, i.e., $\langle\sigma_3\rangle = \langle\sigma_4\rangle = \langle\sigma_5\rangle = 0$. Besides, the mean electric field $\langle\mathbf{E}\rangle$ in the ferroelectric layer may be set equal to the field $\mathbf{E}_0$ induced between metallic electrodes, because the effects due to imperfect compensation of polarization charges by free charge carriers at the ferroelectric/metal interfaces[27] are certainly negligible in the considered range of film thicknesses. (Since the mean

depolarizing field in the film is set to zero, there is no driving force for the formation of purely ferroelectric 180° stripe domains[28] in our case.)

The introduced macroscopic boundary conditions may be supplemented with the microscopic conditions which must be fulfilled on the domain walls. In the rotated reference frame (x_1', x_2', x_3') with the x_3' axis orthogonal to these walls, the condition of strain compatibility in the neighboring domains takes the form $S_{1'}' = S_{1'}''$, $S_{2'}' = S_{2'}''$, and $S_{6'}' = S_{6'}''$. The mechanical equilibrium of the polydomain layer implies that the mechanical stresses in these domains are interrelated as $\sigma_{3'}' = \sigma_{3'}''$, $\sigma_{4'}' = \sigma_{4'}''$, and $\sigma_{5'}' = \sigma_{5'}''$. Finally, the continuity of the tangential components of the internal electric field and the normal component of the electric displacement yields $E_{1'}' = E_{1'}''$, $E_{2'}' = E_{2'}''$, and $\epsilon_0 E_{3'}' + P_{3'}' = \epsilon_0 E_{3'}'' + P_{3'}''$. Thus, in total we have eighteen relationships, which enable us to calculate the internal stresses σ_n', σ_n'' and electric fields E_i', E_i'' in domains of two types as functions of the polarization components P_i', P_i'' and the relative domain population ϕ.

The resulting expression for the mean energy density $\langle \widetilde{F} \rangle$ in a polydomain film makes it possible to perform the numerical minimization of $\langle \widetilde{F} \rangle$ with respect to the remaining seven variables, P_i', $P_i''(i=1,2,3)$, and ϕ. This procedure specifies the equilibrium polarizations inside the domains of the first and second type and their equilibrium volume fractions for a given orientation of the domain walls. Evidently, the calculated energetically favorable polarization configuration depends on the misfit strain S_m in the film-substrate system, temperature T, and the external electric field $\mathbf{E}_0$. However, in the approximation of a dense domain structure, the polarization state appears to be independent of the film thickness.

Using the described thermodynamic approach, the misfit strain-temperature phase diagrams of short-circuited ($\mathbf{E}_0 = 0$) PZT films can be developed, which show the stability ranges of different equilibrium states in the (S_m, T) plane. To this end, the minimum energies $\langle \widetilde{F} \rangle^*(S_m, T, \mathbf{E}_0 = 0)$ of various possible polydomain states should be calculated numerically and compared with each other in order to determine the energetically most favorable one. The comparison with the energies of single-domain PZT films, which were calculated in Ref. 15, must be done in the course of these calculations as well. We recall that only the paraelectric phase ($P_1 = P_2 = P_3 = 0$), the c phase ($P_1 = P_2 = 0$, $P_3 \neq 0$), the aa phase ($|P_1| = |P_2| \neq 0$, $P_3 = 0$), and the r phase ($|P_1| = |P_2| \neq 0$, $P_3 \neq 0$) may be stable in single-domain PZT films in the discussed range of compositions and temperatures.

III. EQUILIBRIUM PHASE DIAGRAMS OF EPITAXIAL PZT FILMS

The thermodynamic calculations of the misfit strain-temperature phase diagrams have been performed for PZT films with the Ti content $x = 0.9$, 0.8, 0.7, 0.6, 0.5, and 0.4. Numerical values of the dielectric stiffnesses α_1, α_{ij}, α_{ijk}, and electrostrictive constants Q_{ln} of the corresponding PZT solid solutions were taken from Ref. 25. The elastic compli-

ances s_{ln} of the paraelectric phase, which are also necessary for the numerical calculations, were evaluated as described in our preceding paper.[15] Three variants of permissible domain-wall orientations in a single-crystalline PZT film have been considered,[20] i.e., the walls parallel to the {101}, {110}, or {100} crystallographic planes of the prototypic cubic phase. Such orientations along the close-packed crystal planes are expected to be energetically favorable due to the interaction of the domain walls with the underlying crystal lattice.[29] It should also be noted that the domain walls with the first orientation are inclined at about 45° to the film-substrate interface, whereas the other two orientations correspond to walls orthogonal to this interface.

Selecting the energetically most favorable thermodynamic state among the polarization configurations allowed for the introduced three domain-wall orientations, we constructed the (S_m, T) phase diagrams of epitaxial PZT films. The developed six diagrams, which correspond to the aforementioned values of the Ti content x in the PZT solid solution, are shown in Fig. 1. We shall discuss below this set of phase diagrams, focusing on the effect of composition on the stability ranges of various possible ferroelectric states.

The inspection of Figs. 1(a)–1(c) shows that the equilibrium diagrams of PZT films with $x \geq 0.7$ are similar to the diagram of PbTiO$_3$ films reported in Ref. 20. They contain only four different stability ranges, which correspond to the paraelectric phase, single-domain ferroelectric c phase, and two polydomain states—pseudotetragonal $c/a/c/a$ and $a_1/a_2/a_1/a_2$ structures (see Fig. 1 in Ref. 20). With the increase of the Zr content, the stability range of the "intermediate" $c/a/c/a$ domain pattern narrows along the misfit-strain axis. The region near $S_m = 0$, where the direct transformation of the paraelectric phase into the $c/a/c/a$ state takes place,[20] becomes very narrow already at $x = 0.9$. In PZT films with $x = 0.7$, this structural transformation occurs only at $S_m = 0$. The stability range of the $c/a/c/a$ pattern is restricted at positive misfit strains by the competition with the $a_1/a_2/a_1/a_2$ polydomain state, which results in a first-order phase transition. At negative misfit strains, this range is bounded by a transition line, where the $c/a/c/a$ state transforms into the homogeneous c phase owing to the complete disappearance of the a domains. This transition is of the second-order in our approximation, but it becomes discontinuous when the self-energies of the domain walls are taken into account.[20]

In contrast, at $x = 0.4$, 0.5, and 0.6, the equilibrium diagram displays a rich variety of stable polarization states. The most remarkable common feature of the (S_m, T) diagrams calculated for these compositions is the presence of at least one *monoclinic* polydomain state. The $r_1/r_2/r_1/r_2$ structure, which represents a polydomain analogue of the monoclinic r phase forming in single-domain PZT films,[15] is common for all three compositions. The field of the $r_1/r_2/r_1/r_2$ pattern grows with the increase of the Zr content in the solid solution [see Figs. 1(d)–1(f)]. In PZT 40/60 and 50/50 thin films, an additional polydomain monoclinic state becomes stable in a narrow range of positive misfit strains. This $ca_1/ca_2/ca_1/ca_2$ state differs from the $r_1/r_2/r_1/r_2$ one by the orientation of the in-plane polarization with respect to the crystal lattice (see Fig. 1 in Ref. 20). Since here the in-plane polarization is
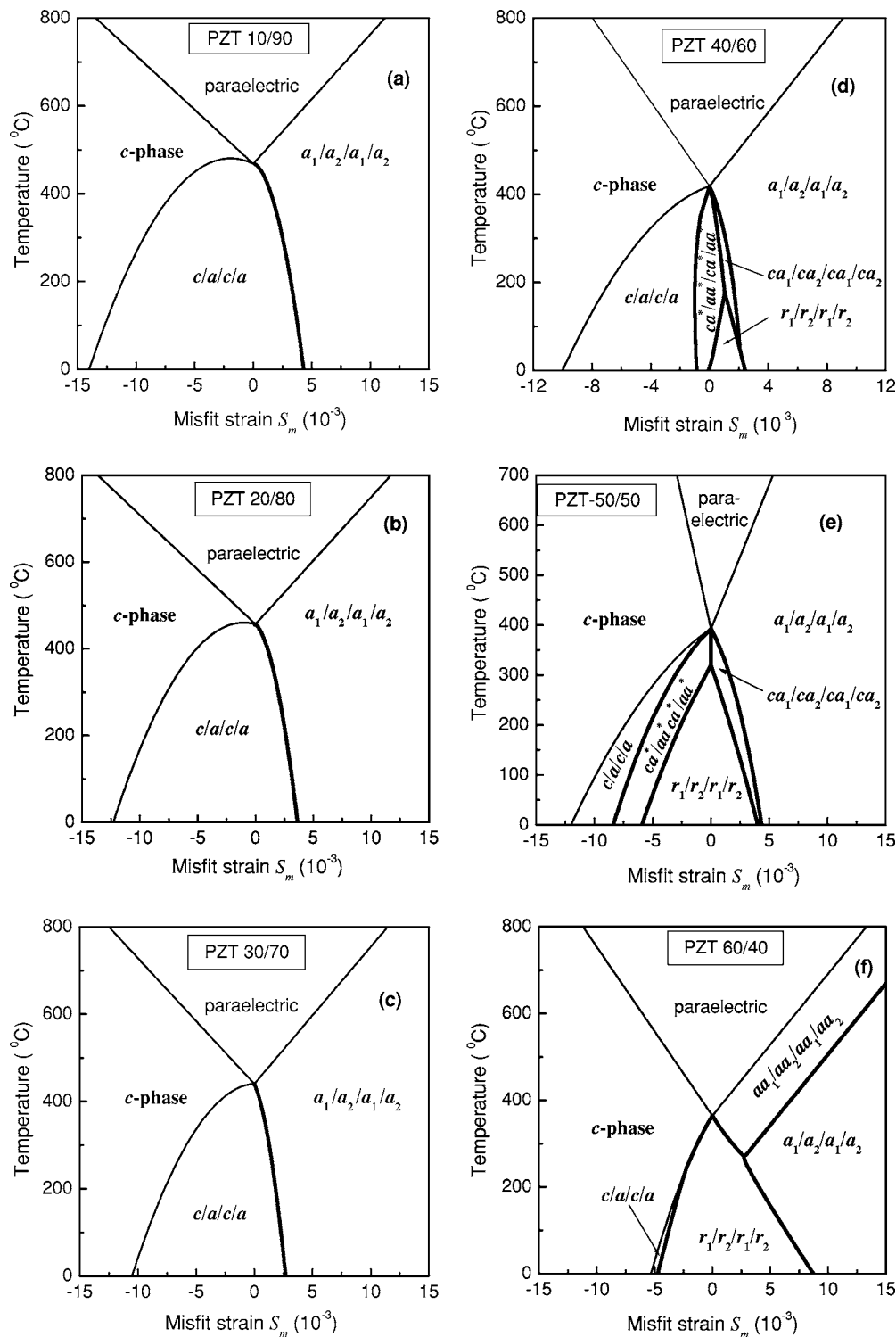
FIG. 1. Phase diagrams of (001)-oriented single-crystalline $Pb(Zr_{1-x}Ti_x)O_3$ films epitaxially grown on dissimilar cubic substrates. The composition x of the solid solution equals 0.9 (a), 0.8 (b), 0.7 (c), 0.6 (d), 0.5 (e), and 0.4 (f). The second- and first-order phase transitions are shown by thin and thick lines, respectively.

parallel to the edge of the prototypic cubic cell, the existence of the $ca_1/ca_2/ca_1/ca_2$ state at $x=0.5$ and 0.6 may be attributed to the fact that these compositions are on the tetragonal side of the bulk morphotropic phase boundary (MPB).[30] It should be noted that the existence of the ca phase in PZT

50/50 films at tensile misfit strains is supported by the results of the first-principles-based simulations.[31]

The equilibrium diagrams of PZT 40/60 and 50/50 films also contain a stability range of the *heterophase* $ca^*/aa^*/ca^*/aa^*$ state. The formation of this polarization
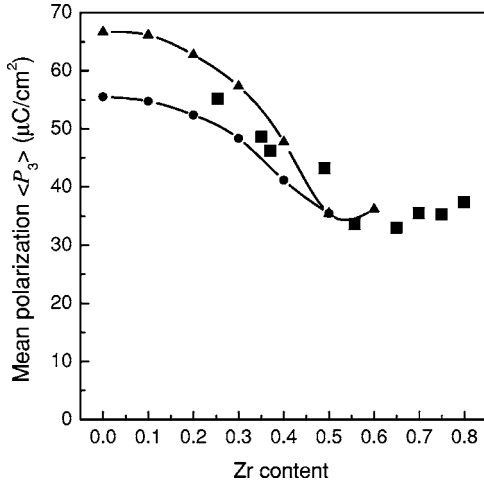
FIG. 2. Mean out-of-plane polarization $\langle P_3 \rangle$ of poled $Pb(Zr_{1-x}Ti_x)O_3$ films at $T = 25$ °C as a function of the Zr content. The misfit strain S_m in the epitaxial system is taken to be -3×10^{-3}, which corresponds to thick PZT films grown on SrTiO₃. Circles and triangles (connected by continuous lines) show the theoretical values calculated for polydomain and single-domain films, respectively. Squares denote the remanent polarization measured by Foster *et al.* (Ref. 6) in submicron-thick PZT films deposited on SrTiO₃ at $T_g = 600$ °C. For the PZT 65/35 film, the remanent polarization is taken from Ref. 31.

configuration is caused by the so-called P_2-instability of the $c/a/c/a$ structure, which leads to the appearance of the in-plane polarization parallel to the domain walls in both c and a domains.[29] The calculations show that the $ca^*/aa^*/ca^*/aa^*$ state formed in PZT films is similar to a heterophase state in the equilibrium diagram of epitaxial BaTiO₃ films.[20] The formation of monoclinic and heterophase states in PZT films greatly reduces the stability range of the $c/a/c/a$ structure near the bulk MPB composition [see Fig. 1(e)].

At $x = 0.4$, when the Zr content exceeds the threshold composition corresponding to that of the bulk MPB ($x = 0.45 - 0.50$), additional qualitative changes of the phase diagram take place. Namely, the field of polydomain states with the in-plane polarization orientation splits into two parts, which correspond to the $a_1/a_2/a_1/a_2$ and $aa_1/aa_2/aa_1/aa_2$ domain configurations. Remarkably, the PZT 60/40 films, unlike epitaxial films of BaTiO₃, PbTiO₃, and other studied PZT solid solutions, exhibit the direct transformation of the paraelectric phase into the orthorhombic $aa_1/aa_2/aa_1/aa_2$ structure at positive misfit strains. At temperatures well below the ferroelectric transition temperature $T_c(S_m)$, however, the $aa_1/aa_2/aa_1/aa_2$ state is replaced by the pseudotetragonal $a_1/a_2/a_1/a_2$ one [Fig. 1(f)]. On the other hand, the stability range of the $c/a/c/a$ structure almost disappears at $x = 0.4$. Finally, it should be noted that, at $S_m = 0$, the direct transformation of the paraelectric phase into the monoclinic $r_1/r_2/r_1/r_2$ polydomain state takes place.

The developed phase diagrams may be used to calculate the misfit-strain and temperature dependences of the average polarization $\langle \mathbf{P} \rangle = \phi^* \mathbf{P}' + (1 - \phi^*) \mathbf{P}''$ in a PZT film and to investigate the influence of composition on the film macro-

scopic polarization state. We determined the effect of the Zr content on the mean out-of-plane polarization $\langle P_3 \rangle$ of poled PZT films grown on SrTiO₃, assuming that the misfit strain in this epitaxial system equals -3×10^{-3}, irrespective of the composition.[15] Figure 2 shows the results of our calculations in comparison with the out-of-plane polarizations P_3 of single-domain PZT films given in Ref. 15. It can be seen that, when the Zr content is less than 0.5, the mean polarization $\langle P_3 \rangle$ of a polydomain film is considerably smaller than the polarization P_3 calculated in the single-domain approximation. This difference is caused by the formation of the $c/a/c/a$ domain structure at $S_m = -3 \times 10^{-3}$, which involves a domains having the in-plane orientation of the spontaneous polarization. In contrast, when the Zr content equals 0.5 or 0.6, $\langle P_3 \rangle$ coincides with the polarization of a single-domain film because the initial $r_1/r_2/r_1/r_2$ state transforms into the homogeneous r phase during the poling.

Our theoretical results may be compared with the compositional variation of the ferroelectric properties, which was observed in submicron-thick PZT films deposited on SrRuO₃ buffered SrTiO₃ crystals.[6] The remanent polarizations of these single-crystalline films, which were measured in a plate-capacitor setup, are also shown in Fig. 2. Evidently, the agreement between theoretical predictions and the experimental data is fairly good. It should be noted, when the Zr content is below 0.4, the experimental points lie between the polarization values predicted for single-domain and polydomain films. This feature probably indicates that the equilibrium volume fraction of c domains in the $c/a/c/a$ structure was not attained in these PZT films due to a finite cooling rate from the deposition temperature.

IV. LATTICE STRAINS AND UNIT-CELL DISTORTIONS IN POLYDOMAIN FILMS

For the better understanding of the microstructure of polydomain ferroelectric films, in this section we consider lattice strains and unit-cell distortions inside domains of the most important types. The in-plane film strains S_1, S_2, S_6 can be calculated from Eqs. (2)–(4), whereas the out-of plane strains are given by[15]

$$S_3 = s_{11}\sigma_3 + s_{12}(\sigma_1 + \sigma_2) + Q_{11}P_3^2 + Q_{12}(P_1^2 + P_2^2), \quad (5)$$

$$S_4 = s_{44}\sigma_4 + Q_{44}P_2 P_3, \quad (6)$$

$$S_5 = s_{44}\sigma_5 + Q_{44}P_1 P_3. \quad (7)$$

For the $c/a/c/a$ state, the stresses involved in Eqs. (2)–(7) can be evaluated as follows. Since the in-plane polarization parallel to the domain walls is absent here ($P_2^a = P_2^c = 0$), the electrostrictive terms $Q_{44}P_1P_2$ and $Q_{44}P_2P_3$ in the equations of state are zero. Therefore, from the macroscopic boundary conditions $\langle \sigma_4 \rangle = 0$ and $\langle \sigma_6 \rangle = 0$ combined with the mechanical conditions fulfilled on the domain walls we obtain $\sigma_4^a = \sigma_4^c = \sigma_6^a = \sigma_6^c = 0$. When the volume fraction of c domains in the film is equal to the equilibrium fraction ϕ_c^*, the polarization vectors inside the c and a domains satisfy additional relationships $|P_1^a| = |P_3^c| = P_s$ and $P_3^a = P_1^c = 0$.[20] Using these
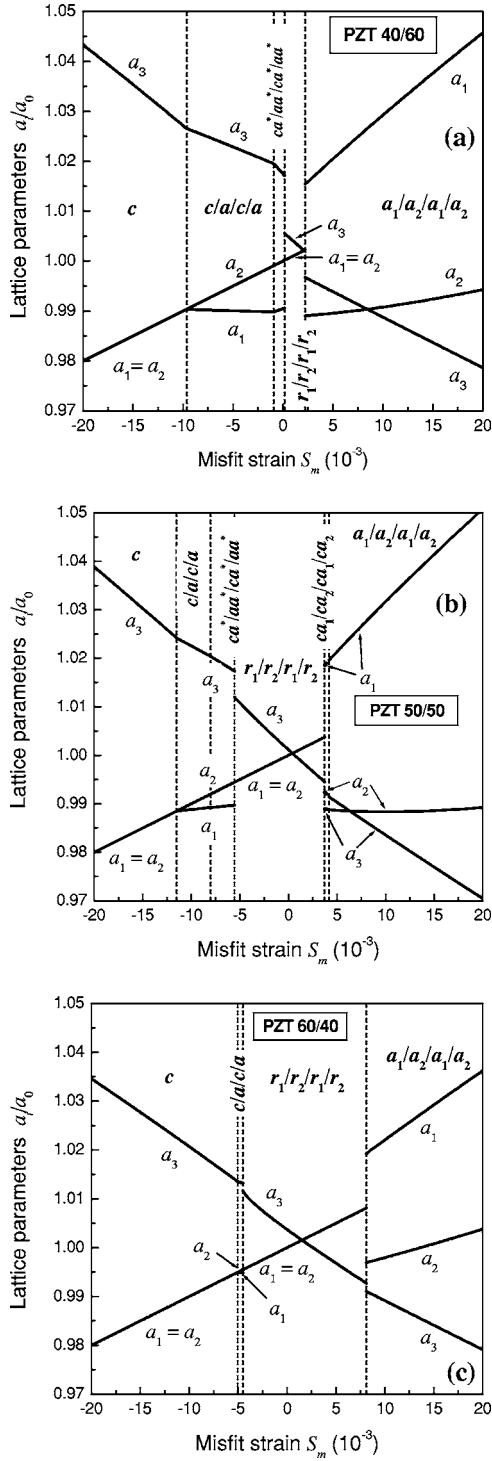
FIG. 3. Out-of-plane (a_3) and in-plane (a_1, a_2) lattice constants in Pb(Zr$_{1-x}$Ti$_x$)O$_3$ films grown on cubic substrates providing different misfit strains S_m in the epitaxial system. The temperature equals 25 °C. For the $c/a/c/a$ and $ca^*/aa^*/ca^*/aa^*$ states, only the lattice parameters in the c and ca^* domains are shown. In the case of the $a_1/a_2/a_1/a_2$ and $ca_1/ca_2/ca_1/ca_2$ structures, the in-plane lattice constants correspond to the a_1 and ca_1 domains, respectively.

equalities, we find that $\sigma_3^a = \sigma_3^c = \sigma_5^a = \sigma_5^c = 0$, $\sigma_1^a = \sigma_1^c = [(s_{11} - s_{12})S_m - (s_{11}Q_{11} - s_{12}Q_{12})P_s^2 + s_{11}(Q_{11} - Q_{12})P_s^2\phi_c^*]/(s_{11}^2 - s_{12}^2)$, and $\sigma_2^a = \sigma_2^c = (S_m - Q_{12}P_s^2 - s_{12}\sigma_1^a)/s_{11}$. The substitution of the

explicit expression for the equilibrium volume fraction ϕ_c^*, which was derived in Ref. 20, further shows that $\sigma_1^a = \sigma_1^c = 0$, i.e., the stress σ_1 completely relaxes due to displacements of ferroelastic domain walls. Hence all internal stresses σ_n are absent in the $c/a/c/a$ structure, except for the stress σ_2 which has the same nonzero value in both domains. Accordingly, the lattice strains can be found from Eqs. (2)–(7) as

$$S_1^a = S_3^c = \frac{s_{12}}{s_{11}}S_m + \left(Q_{11} - \frac{s_{12}}{s_{11}}Q_{12}\right)P_s^2, \qquad (8)$$

$$S_2^a = S_2^c = S_m, \qquad (9)$$

$$S_3^a = S_1^c = \frac{s_{12}}{s_{11}}S_m + \left(1 - \frac{s_{12}}{s_{11}}\right)Q_{12}P_s^2, \qquad (10)$$

$$S_4^a = S_4^c = S_5^a = S_5^c = S_6^a = S_6^c = 0. \qquad (11)$$

It can be seen that there are no shear strains in the film. Besides, the normal strains measured in the directions parallel or orthogonal to the polarization vector coincide in the c and a domains. Therefore, the unit cells inside these domains have the same shape and size, differing by the cell orientation with respect to the film surfaces only. Variations of the lattice constants a_i ($i=1,2,3$) with the misfit strain S_m in an epitaxial system are plotted in Fig. 3 for PZT films of three representative compositions. Remarkably, the lattice parameters measured along the [100] and [010] crystallographic axes, which are perpendicular to the spontaneous polarization, differ from each other in the whole stability range of the $c/a/c/a$ pattern. The crystal lattice in the c and a domains, therefore, is always orthorhombic ($S_1^c \neq S_2^c$ and $S_2^a \neq S_3^a$), but not tetragonal, as assumed in some former papers.[23,24] The $c/a/c/a$ state might be also termed pseudotetragonal in view of its relation to the tetragonal phase of a bulk material.

The $a_1/a_2/a_1/a_2$ domain configuration is characterized by the polarization patterning along the in-plane edges of the prototypic unit cell. As shown in Ref. 20, only the stresses σ_1 and σ_2 differ from zero in this polydomain state, where the spontaneous polarization has the same magnitude P_s in the a_1 ($|P_1^{a_1}|=P_s$, $P_2^{a_1}=0$) and a_2 ($P_1^{a_2}=0$, $|P_2^{a_2}|=P_s$) domains. For the lattice strains inside these domains, the calculation gives

$$S_1^{a_1} = S_2^{a_2} = S_m + \frac{1}{2}(Q_{11} - Q_{12})P_s^2, \qquad (12)$$

$$S_2^{a_1} = S_1^{a_2} = S_m - \frac{1}{2}(Q_{11} - Q_{12})P_s^2, \qquad (13)$$

$$S_3^{a_1} = S_3^{a_2} = \frac{2s_{12}}{s_{11} + s_{12}}S_m + \frac{Q_{12}s_{11} - Q_{11}s_{12}}{s_{11} + s_{12}}P_s^2, \qquad (14)$$

$$S_4^{a_1} = S_4^{a_2} = S_5^{a_1} = S_5^{a_2} = S_6^{a_1} = S_6^{a_2} = 0. \qquad (15)$$

Equations (12)–(14) show that the in-plane strains S_1 and S_2 are distributed inhomogeneously in the $a_1/a_2/a_1/a_2$ polydomain state, whereas the out-of-plane strain S_3 is uniform. The unit cell has the same shape and size inside the a_1 and a_2

domains, but its in-plane orientation in these domains differs by 90°. From the misfit-strain dependence of the lattice constants a_i (see Fig. 3) it follows that, in general, the crystal lattice in the a_1 and a_2 domains has an orthorhombic symmetry. However, at some specific value of S_m, the unit-cell sizes in the crystallographic directions orthogonal to the spontaneous polarization acquire the same value so that the $a_1/a_2/a_1/a_2$ state becomes a tetragonal one. This situation takes place in the PZT 40/60 films at $S_m \cong 8.45 \times 10^{-3}$ and in the PZT 50/50 films at $S_m \cong 6.3 \times 10^{-3}$, but it does not occur in the PZT 60/40 films within the stability range of the $a_1/a_2/a_1/a_2$ structure (see Fig. 3).

The monoclinic $r_1/r_2/r_1/r_2$ state is distinguished from the $c/a/c/a$ and $a_1/a_2/a_1/a_2$ domain configurations by the presence of nonzero shear strains in the film. This feature stems from the fact that here all three polarization components P_i differ from zero in the crystallographic reference frame [see Eqs. (4), (6), and (7)]. In the equilibrium, out-of-plane polarization components in the r_1 and r_2 domains are related as $P_3^{r_1} = -P_3^{r_2}$, and the shear stresses σ_4 and σ_5 are absent. Therefore, the shear strain S_4 is uniform in polydomain films, where the r_1/r_2 domain walls are parallel to the {100} crystallographic planes so that $P_1^{r_1} = P_1^{r_2}$ and $P_2^{r_1} = -P_2^{r_2}$. At the same time, the strain S_5 changes the sign on crossing the domain walls. Taking into account other results of our numerical calculations, we can describe the strain state of a film with the $r_1/r_2/r_1/r_2$ structure by the following set of equalities:

$$S_1^{r_1} = S_2^{r_1} = S_1^{r_2} = S_2^{r_2} = S_m, \tag{16}$$

$$S_3^{r_1} = S_3^{r_2}, \tag{17}$$

$$S_4^{r_1} = -S_5^{r_1} = S_4^{r_2} = S_5^{r_2}, \tag{18}$$

$$S_6^{r_1} = -S_6^{r_2}. \tag{19}$$

Variations of the lattice constants a_i in the r_1 and r_2 domains with the misfit strain at room temperature are shown in Fig. 3. The in-plane lattice parameters a_1 and a_2 have the same magnitude in these domains, whereas the out-of-plane parameter a_3 generally differs from $a_1 = a_2$. This result clearly shows that the crystal lattice in the $r_1/r_2/r_1/r_2$ state is not normally rhombohedral, in contrast to the assumption made in the linear theory.[32,33] The lattice in the r_1 and r_2 domains becomes rhombohedral only at a special value of the misfit strain, which depends on the composition and equals $S_m \cong 2.12 \times 10^{-3}$, 4×10^{-4}, and 1.5×10^{-3} for the PZT 40/60, 50/50, and 60/40 films, respectively. It should be noted that in the linear theory the spontaneous polarization $\mathbf{P}_s$ was supposed to be oriented along the cube diagonal of the prototypic unit cell,[32] whereas actually the orientation of $\mathbf{P}_s$ in the $r_1/r_2/r_1/r_2$ structure varies with the misfit strain.[20]

V. DIELECTRIC RESPONSE OF EPITAXIAL PZT FILMS

Determination of the dielectric and piezoelectric responses of polydomain films to the application of an external
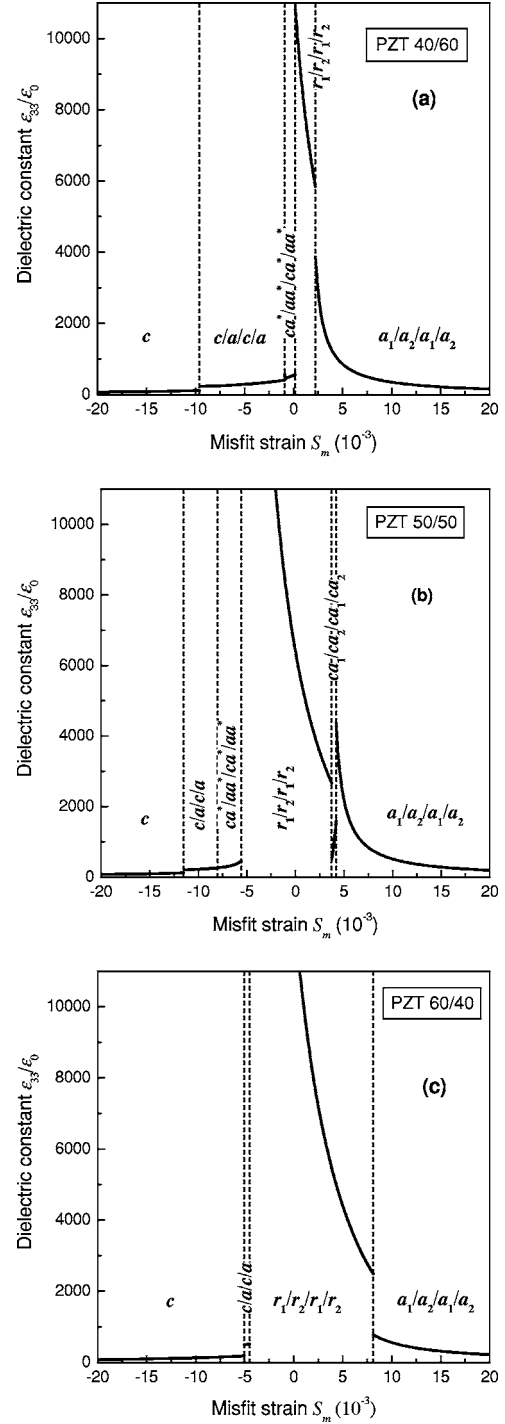

FIG. 4. Out-of-plane dielectric response ε_{33} of epitaxial Pb(Zr$_{1-x}$Ti$_x$)O$_3$ films calculated as a function of the misfit strain at $T = 25\,°C$. The composition x of the solid solution equals 0.6 (a), 0.5 (b), and 0.4 (c).

field is generally complicated by the presence of an extrinsic contribution caused by field-induced displacements of domain walls.[20] When this contribution differs from zero, the film material constants can be calculated only numerically, because the wall displacements alter not only volumes of adjacent domains, but also polarizations and lattice strains inside them. In order to evaluate the dielectric response, for

instance, the film average polarization $\langle \mathbf{P} \rangle$ should be computed as a function of the external electric field $\mathbf{E}_0$. The small-signal dielectric constants $\varepsilon_{ij}(\mathbf{E}_0 \rightarrow 0)$ can be found then from the formula

$$\epsilon_{ij} = \frac{\langle P_i \rangle (E_{0j} = E_0) - \langle P_i \rangle (E_{0j} = 0)}{E_0}, \qquad (20)$$

where the field intensity E_0 must correspond to the linear part of the dependence $\langle \mathbf{P} \rangle (\mathbf{E}_0)$.

Using Eq. (20), we have performed numerical calculations of the out-of-plane permittivity ε_{33}, which is measured in a conventional plate-capacitor setup. Figure 4 shows the misfit-strain dependence of ε_{33} at room temperature for PZT films with the Ti content $x = 0.6$, 0.5, and 0.4. The most remarkable theoretical result relates to the behavior of the monoclinic $r_1/r_2/r_1/r_2$ state. For all studied compositions, the film dielectric response $\varepsilon_{33}(S_m)$ reaches its maximum value within the stability range of this polydomain state, where the relative permittivity may exceed 10^4. It should be noted, however, that in the case of the $r_1/r_2/r_1/r_2$ structure the domain-wall contribution to the permittivity is large. (Since the out-of-plane polarization component P_3 differs in sign in the r_1 and r_2 domains, the electric field in a plate-capacitor setup creates considerable driving force acting on the r_1/r_2 walls.) Therefore, our theory probably overestimates the dielectric response of conventional (imperfect) PZT films, where crystal defects may create additional restoring forces hindering the motion of the domain walls.

A steplike increase of the permittivity at the transformation of the c phase into the $c/a/c/a$ state, which is clearly seen in Fig. 4, is also associated with the domain-wall contribution. This contribution to the out-of-plane dielectric response ε_{33} equals zero in a polydomain single-crystalline film only when the domain structure is of the $a_1/a_2/a_1/a_2$ type. The characteristic feature of the $a_1/a_2/a_1/a_2$ state is the increase of the dielectric response with a decreasing positive misfit strain S_m (Fig. 4), which is caused by the P_3 instability of this polarization configuration.[34] The analysis shows that the inverse of the film permittivity, $1/\varepsilon_{33}$, varies with S_m almost linearly in the stability range of the $a_1/a_2/a_1/a_2$ structure. This *Curie-Weiss-type law* for the strain effect on the out-of-plane dielectric response of ferroelectric films, which was formulated in Ref. 35, also holds within the stability range of the c phase.

In conclusion of this section we recall that the field-induced displacements Δl of the domain walls are additionally hindered by the lattice potential barriers.[36] For ferroelastic domain walls considered in the present paper, these so-called Peierls barriers are expected to be small since the thickness of a ferroelastic wall is usually much larger than the lattice period a.[37] Nevertheless, the Peierls potential relief will limit the increase of the domain-wall contribution in the situations, where other restoring forces acting on the walls become negligible. Approximating the lattice potential relief $U(\Delta l)$ by the relation $U = U_0 [1 - \cos(2\pi \Delta l / a)]/2$, we can evaluate the maximum domain-wall contribution as

$$\Delta \varepsilon_{33}^{\max} \cong \frac{\delta P_3^2 a^2}{\pi^2 U_0 D}, \qquad (21)$$

where δP_3 is the change of the polarization component P_3 in the volume swept by the wall, and D is the period of the laminar domain structure. [In accordance with the numerical estimates, the wall displacement $\Delta l \cong \delta P_3 E_3 a^2 / (2\pi^2 U_0)$ in a weak electric field $E_3 \sim 10^3$ V/m used in the dielectric measurements is taken to be much smaller than the lattice period.] Unfortunately, the Peierls barrier U_0 is unknown for the domain walls in PZT. At the same time, the results of a first-principles study[36] of the energetics of 90° domain walls in PbTiO$_3$ indicate that, at low temperatures, the interaction with the crystal lattice may reduce the domain-wall contribution considerably. Indeed, taking $U_0 = 1.6$ mJ/m^2 (Ref. 36), $\delta P_3 = P_s = 0.75$ C/m^2, $a = 0.4$ nm and assuming $D \sim 10$ nm, from Eq. (21) we obtain $\Delta \varepsilon_{33}^{\max} / \varepsilon_0 \sim 50$. Furthermore, the Peierls barrier for purely ferroelectric 180° domain walls was found to be much larger than for ferroelastic/ferroelectric 90° walls.[36] For the 180° walls in PbTiO$_3$ ($U_0 = 37$ mJ/m^2, $\delta P_3 = 2P_s = 1.5$ C/m^2) and BaTiO$_3$ ($U_0 = 9.3$ mJ/m^2, $\delta P_3 = 2P_s = 0.52$ C/m^2), Eq. (21) gives $\Delta \varepsilon_{33}^{\max} / \varepsilon_0 \sim 10$ and 5, respectively. These small values demonstrate that a very large dielectric response of ferroelectric films with thin dead layers, which was predicted in Ref. 38, cannot be observed in PbTiO$_3$ and BaTiO$_3$ films.

VI. CONCLUSIONS

Our thermodynamic calculations demonstrate that the composition of the solid solution has a strong impact on the phase diagrams of epitaxial PZT films. At the Zr content less than 0.4, the misfit strain-temperature diagrams of PZT films are characterized by the presence of a large stability range of the $c/a/c/a$ state near $S_m = 0$ at room temperature. In contrast, in PZT 50/50 and 60/40 films, the field of this state is replaced to a great extent by the stability range of the $r_1/r_2/r_1/r_2$ domain pattern. Besides, the paraelectric to ferroelectric phase transition, at positive misfit strains, leads to the appearance of the orthorhombic $aa_1/aa_2/aa_1/aa_2$ state in PZT 60/40 films, whereas in the other studied PZT solid solutions it results in the formation of the pseudo-tetragonal $a_1/a_2/a_1/a_2$ configuration.

Comparison of the phase diagrams shown in Fig. 1 with the diagrams of single-domain PZT films[15] also demonstrates that the strain relaxation caused by the twinning of an epitaxial layer may change the polarization state of a PZT film considerably. For instance, the orthorhombic aa phase forming in single-domain films at large positive misfit strains[15] is replaced by the $a_1/a_2/a_1/a_2$ domain structure so that the polarization becomes oriented along the in-plane edges of the unit cell instead of its face diagonal. At the Zr content less than 0.4, the twinning also removes the monoclinic phase from the (S_m, T) diagram of PZT films. However, the prediction concerning the formation of a monoclinic state[15] remains valid for PZT films with the Zr content equal or larger than 0.4. The monoclinic $r_1/r_2/r_1/r_2$ domain pattern is expected to form, for instance, in thick PZT films that are grown on SrTiO$_3$ ($S_m \approx -3 \times 10^{-3}$) and have $x \lesssim 0.5$ [see Fig.

1(e) and 1(f)]. This prediction is supported by the experimental results obtained by Streiffer *et al.*[32] for the PZT 65/35 film deposited on SrTiO₃. Indeed, the twin walls observed in this film are parallel to the crystallographic (100) or (010) planes, as characteristic of the r_1/r_2 walls, and the measured remanent polarization is rather close to the theoretical value calculated for PZT 60/30 film (see Fig. 2).

The dielectric properties of epitaxial PZT films are sensitive to the strain relaxation as well. The dielectric anomaly, which is displayed by single-domain PZT films at $S_m \sim 10^{-2}$, disappears in polydomain (twinned) films. Nevertheless, the out-of-plane permittivity ε_{33} of a polydomain PZT film may reach very large values exceeding 10^4. This dielectric anomaly may be observed in PZT films with the $r_1/r_2/r_1/r_2$ domain structure in the absence of the domain-wall pinning by crystallographic defects.

*Corresponding author. Electronic address: pertsev@domain.ioffe.rssi.ru

[1] J. Lee, A. Safari, and R. L. Pfeffer, Appl. Phys. Lett. **61**, 1643 (1992).

[2] R. Ramesh, T. Sands, and V. G. Keramidas, Appl. Phys. Lett. **63**, 731 (1993).

[3] M. de Keijser, J. F. M. Cillessen, R. B. F. Janssen, A. E. M. De Veirman, and D. M. de Leeuw, J. Appl. Phys. **79**, 393 (1996).

[4] J.-M. Triscone, L. Frauchiger, M. Decroux, L. Miéville, Ø. Fisher, C. Beeli, P. Stadelmann, and G.-A. Racine, J. Appl. Phys. **79**, 4298 (1996).

[5] T. Yu, Y.-F. Chen, Z.-G. Liu, S.-B. Xiong, L. Sun, X.-Y. Chen, L.-J. Shi, and N.-B. Ming, Appl. Phys. Lett. **69**, 2092 (1996).

[6] C. M. Foster, G.-R. Bai, R. Csencsits, J. Vetrone, R. Jammy, L. A. Wills, E. Carr, and J. Amano, J. Appl. Phys. **81**, 2349 (1997).

[7] T. Tybell, C. H. Ahn, and J.-M. Triscone, Appl. Phys. Lett. **75**, 856 (1999).

[8] V. Nagarajan, I. G. Jenkins, S. P. Alpay, H. Li, S. Aggarval, L. Salamanca-Riba, A. L. Roytburd, and R. Ramesh, J. Appl. Phys. **86**, 595 (1999).

[9] O. Kuffer, I. Maggio-Aprile, J.-M. Triscone, Ø. Fisher, and Ch. Renner, Appl. Phys. Lett. **77**, 1701 (2000).

[10] K. Nagashima, M. Aratani, and H. Funakubo, J. Appl. Phys. **89**, 4517 (2001).

[11] C. L. Jia, J. Rodríguez Contreras, U. Poppe, H. Kohlstedt, R. Waser, and K. Urban, J. Appl. Phys. **92**, 101 (2002).

[12] J. Rodríguez Contreras, H. Kohlstedt, U. Poppe, R. Waser, and Ch. Buchal, Appl. Phys. Lett. **83**, 126 (2003).

[13] K. Saito, T. Kurosawa, T. Akai, T. Oikawa, and H. Funakubo, J. Appl. Phys. **93**, 545 (2003).

[14] S. H. Oh and H. M. Jang, Appl. Phys. Lett. **72**, 1457 (1998); Phys. Rev. B **62**, 14757 (2000); **63**, 132101 (2001).

[15] N. A. Pertsev, V. G. Kukhar, H. Kohlstedt, and R. Waser, Phys. Rev. B **67**, 054107 (2003).

[16] L. Chen, V. Nagarajan, R. Ramesh, and A. L. Roytburd, J. Appl. Phys. **94**, 5147 (2003).

[17] Y. L. Li, S. Choudhury, Z. K. Liu, and L. Q. Chen, Appl. Phys. Lett. **83**, 1608 (2003).

[18] Y. L. Li, S. Y. Hu, Z. K. Liu, and L. Q. Chen, Appl. Phys. Lett. **78**, 3878 (2001).

[19] N. A. Pertsev, A. G. Zembilgotov, and A. K. Tagantsev, Phys. Rev. Lett. **80**, 1988 (1998); Ferroelectrics **223**, 79 (1999).

[20] V. G. Koukhar, N. A. Pertsev, and R. Waser, Phys. Rev. B **64**, 214103 (2001).

[21] A. L. Roitburd, Phys. Status Solidi A **37**, 329 (1976).

[22] B. S. Kwak, A. Erbil, B. J. Wilkens, J. D. Budai, M. F. Chisholm, and L. A. Boatner, Phys. Rev. Lett. **68**, 3733 (1992).

[23] W. Pompe, X. Gong, Z. Suo, and J. S. Speck, J. Appl. Phys. **74**, 6012 (1993).

[24] N. A. Pertsev and A. G. Zembilgotov, J. Appl. Phys. **78**, 6170 (1995); **80**, 6401 (1996).

[25] M. J. Haun, E. Furman, S. J. Jang, and L. E. Cross, Ferroelectrics **99**, 13 (1989).

[26] D. Vanderbilt and M. H. Cohen, Phys. Rev. B **63**, 094108 (2001).

[27] R. R. Mehta, B. D. Silverman, and J. T. Jacobs, J. Appl. Phys. **44**, 3379 (1973); D. R. Tilley and B. Žekš, Ferroelectrics **134**, 313 (1992); J. Junquera and Ph. Ghosez, Nature (London) **422**, 506 (2003); Na Sai, A. M. Kolpak, and A. M. Rappe, Phys. Rev. B **72**, 020101(R) (2005).

[28] D. D. Fong, G. B. Stephenson, S. K. Streiffer, J. A. Eastman, O. Auciello, P. H. Fuoss, and C. Thompson, Science **304**, 1650 (2004).

[29] N. A. Pertsev and V. G. Koukhar, Phys. Rev. Lett. **84**, 3722 (2000).

[30] B. Jaffe, W. R. Cook, and H. Jaffe, *Piezoelectric Ceramics* (Academic, London, 1971).

[31] I. Kornev, H. Fu, and L. Bellaiche, Phys. Rev. Lett. **93**, 196104 (2004).

[32] S. K. Streiffer, C. B. Parker, A. E. Romanov, M. J. Lefevre, L. Zhao, J. S. Speck, W. Pompe, C. M. Foster, and G. R. Bai, J. Appl. Phys. **83**, 2742 (1998).

[33] A. E. Romanov, M. J. Lefevre, J. S. Speck, W. Pompe, S. K. Streiffer, and C. M. Foster, J. Appl. Phys. **83**, 2754 (1998).

[34] V. G. Koukhar, N. A. Pertsev, and R. Waser, Appl. Phys. Lett. **78**, 530 (2001).

[35] N. A. Pertsev, V. G. Koukhar, R. Waser, and S. Hoffmann, Appl. Phys. Lett. **77**, 2596 (2000).

[36] B. Meyer and D. Vanderbilt, Phys. Rev. B **65**, 104111 (2002).

[37] J. Chrosch and E. K. H. Salje, J. Appl. Phys. **85**, 722 (1999).

[38] A. M. Bratkovsky and A. P. Levanyuk, Phys. Rev. B **63**, 132103 (2001).